AEGC Australasian Exploration Geoscience Conference Brisbane 2021

Automated fracture detection and characterization from unwrapped drill-core images using Mask R-CNN

Fatimah Alzubaidi[1]
f.al-zubaidi@unsw.edu.au

Patrick Makuluni[1]
p.makuluni@unsw.edu.au

Stuart R. Clark[1]
stuart.clark@unsw.edu.au

Jan Erik Lie[2]
jan-erik.lie@lundin-energy.com

Peyman Mostaghimi[1]
peyman@unsw.edu.au

Ryan T. Armstrong[1]
ryan.armstrong@unsw.edu.au

[1]School of Minerals and Energy Resources, University of New South Wales, Sydney, Australia.

[2] Lundin Energy Norway AS, Lysaker, Norway

SUMMARY

Drill cores provide the most reliable fracture information in subsurface formations as they present a clear and direct view of fractures. Core observation and image log interpretation are usually integrated for fracture analysis of underground layers. There has been a strong move towards developing automated fracture detection methods, however, the focus has been on extracting fracture information from log images, such as acoustic or resistivity image logs. Such efforts using core images are significantly less. This study presents a machine learning-based approach for automatic fracture recognition from unwrapped drill-core images. The proposed method applies a state-of-the-art convolutional neural network for object identification and segmentation. The study also investigates the feasibility of using synthetic fracture images for training the model by creating two types of synthetic data using masks of real fractures and creating sinusoidal shaped fractures. The trained model is then used to detect fractures in real core images from two different boreholes and achieved a precision of 94.80%. The identified fractures are further analyzed and compared to manually segmented fractures in terms of fracture dip angle and dip direction, which achieved average absolute errors of 2.18° and 10.58°, respectively. Overall, the study presents a novel application of an advanced machine learning algorithm for fracture detection and analysis from unwrapped core images.

Key words: unwrapped core images, mask R-CNN, fracture detection, fracture analysis

INTRODUCTION

Fracture analysis for subsurface formations is crucial in many geological, geotechnical and petroleum related applications. It is important for geological modelling, oil and gas reservoir characterization, borehole stability, and assessing rock quality for subsurface engineering. Fracture analysis is performed based on information obtained from well log data and drill cores (Nian *et al.*, 2016; Fernández-Ibáñez, DeGraff and Ibrayev, 2018; Lai *et al.*, 2021). The conventional procedure of fracture analysis is laborious and time-consuming, therefore, there is a need for fast and reliable approaches to automate it.

Drill cores provide accurate and reliable fracture analysis Fernández-Ibáñez *et al.* (2018) as they present a detailed and direct view of fractures. With the recent trend towards digital archiving of core data (Betlem *et al*., 2020; Tiwari *et al*., 2017); fractures can be identified from the digital images of cores. The unwrapped core images, in particular, show detailed fracture features of the entire core. Studies based on analyzing unwrapped core images are limited although they provide valuable fracture information.

Previous attempts to identify fractures–such as Lemy *et al.* (2001) and Ozturk and Saricam (2018)–used core tray images that show the core from only one angle, moreover, the methods were based on image processing methods that have limited generalization and robustness.

In this work, we demonstrate an innovative approach for fracture characterization whereby a Mask R-CNN model (He *et al.*, 2017) was used for fracture detection from unwrapped core images. We used the model to detect and segment fractures in core images. We then fit a sine wave to the detected fracture points to obtain depth, dip angle and dip direction. We tested the model on 88 m of core from two boreholes; the total processing time was 5 minutes. Our calculations assumed a case of a vertical core where the objective was to compare the model results to those from manual detection whereas providing a geological interpretation of the region was beyond our scope.

METHOD AND RESULTS

Data preparation

The data included unwrapped core images from two boreholes and synthetic fractured-core images created with two types of fractures (Table 1). We obtained the unwrapped core images from Lundin Energy company, Lysaker, Norway. We created the synthetic data by adding fracture masks to background images of cores with no fracture, using fracture masks obtained from shapes of real fractures and from a sine function. We created the training dataset mainly (~94%) from synthetic images and used the majority of the real images for testing.

Table 1. Number and type of images used in building and testing the model, including images with two types of synthetic fractures.

Image by fracture type	Training dataset	Validation dataset	test dataset
Real fractures	62	35	88 m
Synthetic fractures A	531	58	
Synthetic fractures B	525	52	
Total No. of images	1,118	145	
Total No. of fractures	1,649	218	243

Methodology

The main steps of our workflow were segmenting fractures in the input images and analyzing the extracted fractures (Figure 1). For fracture segmentation, we used Mask R-CNN (He *et al*., 2017), which is a state-of-art instance segmentation model extended from Faster R-CNN (Girshick, 2015). Mask R-CNN predicts a category, bounding box, and a segmented binary mask for each object in the input image. In our work, we relied on the binary masks to extract fracture details.

To apply the model on our fracture dataset, we modified several structure and training parameters. We increased the size of the input images to have 2000 pixels on the large edge, instead of the default size of 1333 pixels. We also modified sizes and height-to-width ratios of the anchors in the region proposal network (RPN). As Mask R-CNN is a region-based model, it uses RPN to propose regions of the image containing candidate objects. We defined large anchors of up to 1024 pixels^2 and height-to-width ratios of 3:4, 1:1, and 2:1. Mask R-CNN uses a deep CNN for feature extraction, called a backbone. We used ResNet-50 with a feature pyramid network (FPN) (Lin *et al*., 2017) as the backbone for our model. During training, the model calculates the loss as a summation of the classification loss, bounding box regression loss, and mask segmentation loss. We multiplied the segmentation loss by a factor of 1.5 to improve the segmentation, as proposed by Xu *et al*. (2020).

We started the training from a pretrained model on the MSCOCO dataset of natural images (Lin *et al*., 2014). To avoid overfitting, we trained the last three blocks of the backbone through four stages for a total of 60 epochs. We used an initial learning rate of 0.005 in the first two stages and a smaller learning rate of 0.001 in the last stages. Other training and structure parameters were according to the default.

The second step of the workflow was estimating fracture depth, dip angle and dip direction using the segmented fracture masks (Figure 1, bottom). The main operations applied on each mask were extracting fracture skeleton, sine wave fitting, and using the parameters of the fitted sine wave to obtain fracture details according to the equations from Elkington and Assous (2017). To accelerate the calculations involved in these operations, we first downsampled the masks by a factor of 0.25. We obtained fracture skeleton using morphological image processing from Scikit-image (Van Der Walt *et al*., 2014). We then fitted skeleton points to a sine wave through two fitting stages with wave lengths of $0.5-2w$ and w, respectively, where w is the mask width. As demonstrated in Figure 1, we obtained fracture location, from the centerline of the fitted wave. We calculated the dip angle from the amplitude of the sine function and core diameter as

$$tan(\theta) = 2A\ \frac{\pi}{w}, \qquad (1)$$

where θ is the dip angle, A the amplitude of the sine wave and w is the mask width.

Finally, we obtained the dip direction from the minimum point of the sine wave (Rider, 1996). We calculated the dip direction only for fractures with more than 5° dip angles; for lower dips the location of the minimum was uncertain especially when the fracture path did not represent a sine wave.

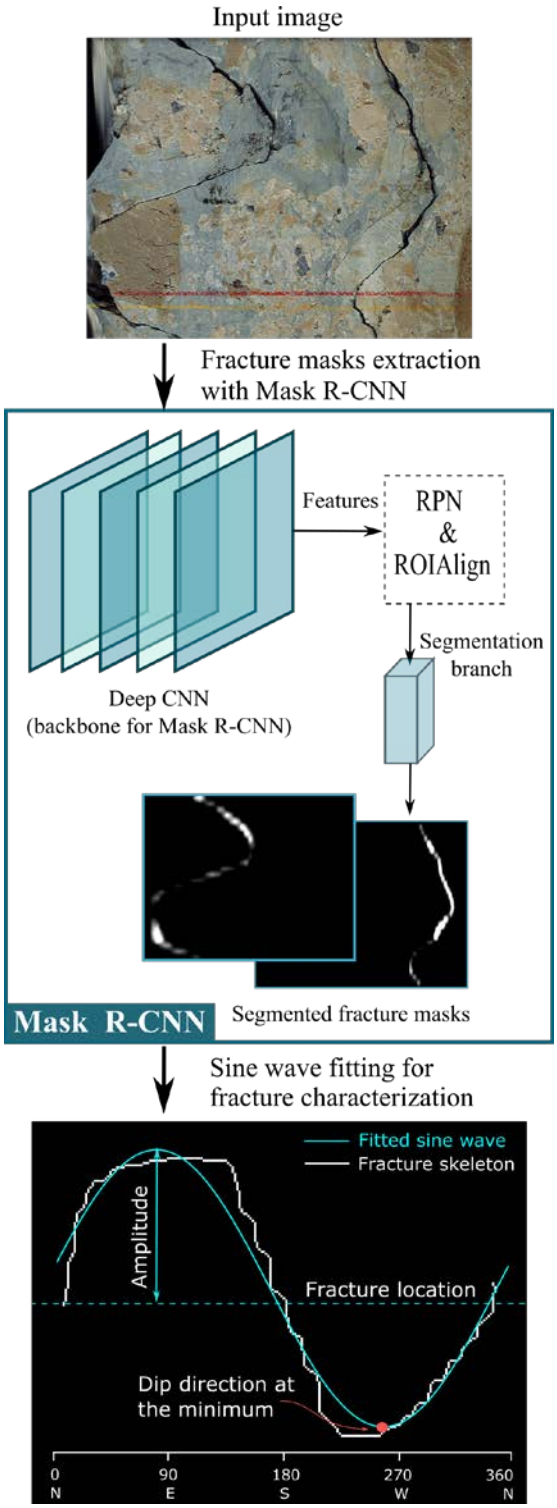

Figure 1. Workflow of the proposed method. Fractures in the unwrapped core image were segmented using Mask R-CNN, and fracture details were calculated by analyzing the segmented fracture masks.

Results

To evaluate the detection results, we first calculated the precision and recall– which are common evaluation metrics for object detection–as below:

$$Precision = \frac{TP}{TP + FP}, \quad (2)$$

$$Recall = \frac{TP}{TP + FN}, \quad (3)$$

where TP, FP, and FN are the numbers of true positives, false positives, and false negatives, respectively. We decided on TP, FP, and FN based on the depths of the detected fractures to those obtained from manual segmentation.

The model achieved accurate detection from the test images of both boreholes despite being trained on synthetic images; it resulted in average precision of 94.80% and average recall of 86.67%. A test image with different factures and its detection results from the model are presented in Figure 2.

Dip angle calculations from both boreholes are shown in Figure 3. They resulted in an average error of 2.18° for a total of 210 detected fractures; approximately 98% of the fractures had errors less than 10°, including 93% with less than 5° errors.

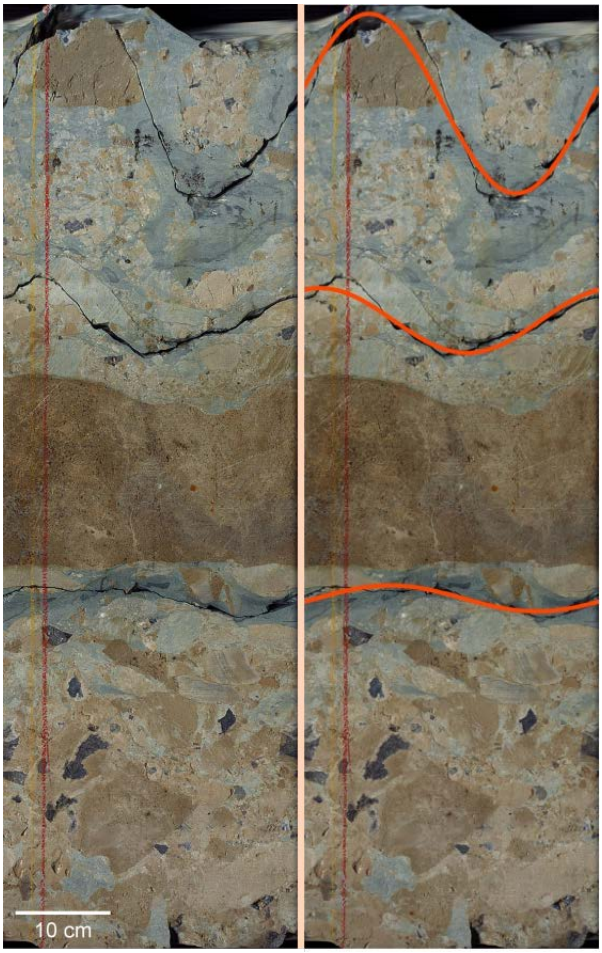

Figure 2. Fracture detection by the model, input image is shown on the left and detected fractures are shown in red on the right.

Dip direction were less accurate than dip angle results, as shown in Figure 3. Because dip directions depend on the minimum of the sine wave, they were highly sensitive to the sine fitting and, in turn, to the fracture segmentation. Consequently, the dip direction calculations obtained average absolute errors of 10.58° for a total of 186 detected fractures from both boreholes; 74% of the fractures had errors less than the average, and only 5% had errors greater than 40°.

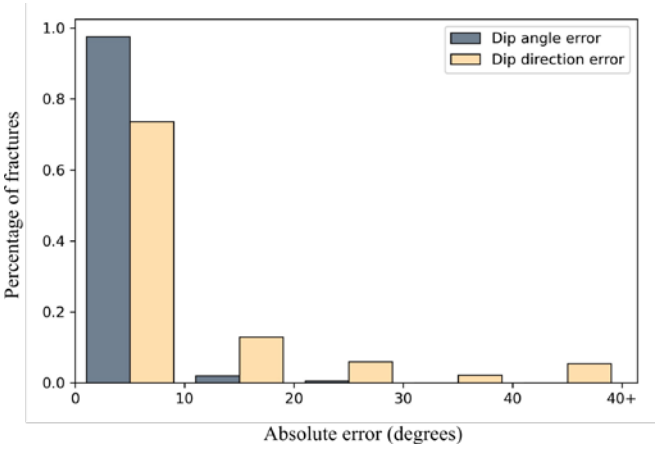

Figure 3. Error analysis for all fractures in the test images based on the results of dip angle and dip direction.

CONCLUSIONS

The study offers a fully automated workflow to provide detailed fracture characterization from unwrapped core images. The workflow was developed based on an advanced machine learning model for instance segmentation, Mask R-CNN.

The model was trained mostly on synthetic data and tested on real core images from two different boreholes. The test images included a total of 88 m of core with 243 fractures. The model achieved average detection precision and recall of 94.80% and 86.67%, respectively. For the characterization of the detected fractures, we relied on the segmented fracture masks by fitting a sine wave to the detected fracture points. The parameters of the resulting sine wave were used to calculate fracture depth, dip angle and dip direction. Fracture characterization achieved excellent results from dip angle calculations with an average absolute error of 2.18° only. Although dip direction had a higher average error of 10.58°, most calculated directions were in agreement with those based on manual segmentation. The total processing time depended on the image resolution, on average it was 4 seconds per meter.

ACKNOWLEDGMENTS

The authors acknowledge the help from Lundin Energy in providing the unwrapped core images used in the study.

REFERENCES

Betlem, P., Birchall, T., Ogata, K., Park, J., Skurtveit, E., & Senger, K., 2020. Digital drill core models: Structure-from-motion as a tool for the characterisation, orientation, and digital archiving of drill core samples. Remote Sensing, 12.

Elkington, P. A. S., & Assous, S., 2017. Methods of and apparatuses for identifying geological characteristics in boreholes (Patent No. US 9,704,263 B2).

Fernández-Ibáñez, F., DeGraff, J. M., & Ibrayev, F., 2018. Integrating borehole image logs with core: A method to enhance subsurface fracture characterization. AAPG Bulletin, 102, 1067–1090.

Girshick, R., 2015. Fast R-CNN. 2015 IEEE International Conference on Computer Vision (ICCV), 2015 Inter, 1440–1448.

He, K., Gkioxari, G., Dollar, P., & Girshick, R., 2017. Mask R-CNN. 2017 IEEE International Conference on Computer Vision, 2961–2969.

Lai, J., Chen, K., Xin, Y., Wu, X., Chen, X., Yang, K., Song, Q., Wang, G., & Ding, X., 2021. Fracture characterization and detection in the deep Cambrian dolostones in the Tarim Basin, China: Insights from borehole image and sonic logs. Journal of Petroleum Science and Engineering, 196.

Lemy, F., Hadjigeorgiou, J., Côté, P., & Maldague, X., 2001. Image analysis of drill core. Mining Technology, 110, 172–177.

Lin, T.-Y., Dollár, P., Girshick, R., He, K., Hariharan, B., & Belongie, S., 2017. Feature Pyramid Networks for Object Detection. Proceedings of the IEEE Conference on Computer Vision and Pattern Recognition, 2117–2125.

Lin, T. Y., Maire, M., Belongie, S., Hays, J., Perona, P., Ramanan, D., Dollár, P., & Zitnick, C. L., 2014. Microsoft COCO: Common objects in context. European Conference on Computer Vision, 8693 LNCS(PART 5), 740–755.

Lundin Energy, n.d.. Retrieved October 14, 2020, from https://www.lundin-energy.com/

Nian, T., Wang, G., Xiao, C., Zhou, L., Sun, Y., & Song, H., 2016. Determination of in-situ stress orientation and subsurface fracture analysis from image-core integration: an example from ultra-deep tight sandstone (BSJQK Formation) in the Kelasu Belt, Tarim Basin. Journal of Petroleum Science and Engineering, 147, 495–503.

Ozturk, H., & Saricam, I. T., 2018. Core Segmentation and Fracture Path Detection Using Shadows. Journal of Image and Graphics, 6, 69–73.

Rider, M. H., 1996. The Geological Interpretation of Well Logs (2nd ed.). Rider-French Consulting Ltd.

Tiwari, S., Mishra, S., Srihariprasad, G., Vyas, D., Warhade, A., Nikalje, D., Bartakke, V., Mahesh, B., Tembhurnikar, P., & Roy, S., 2017. High resolution core scan facility at BGRL-MoES, Karad, India. Journal of the Geological Society of India, 90, 795–797.

Van Der Walt, S., Schönberger, J. L., Nunez-Iglesias, J., Boulogne, F., Warner, J. D., Yager, N., Gouillart, E., & Yu, T., 2014. Scikit-image: Image processing in python. PeerJ, 2014(1), e453.

Xu, S., Lan, S., & Zhu, Q., 2020. MaskPlus: Improving mask generation for instance segmentation. Proceedings - 2020 IEEE Winter Conference on Applications of Computer Vision, 2019–2027.